

## Multiple time scale molecular dynamics for fluids with orientational degrees of freedom. I. Microcanonical ensemble

Igor P. Omelyan and Andriy Kovalenko

Citation: *J. Chem. Phys.* **135**, 114110 (2011); doi: 10.1063/1.3637035

View online: <http://dx.doi.org/10.1063/1.3637035>

View Table of Contents: <http://jcp.aip.org/resource/1/JCPSA6/v135/i11>

Published by the [American Institute of Physics](#).

---

### Related Articles

Monte Carlo study of four dimensional binary hard hypersphere mixtures

*J. Chem. Phys.* **136**, 014506 (2012)

Energy relaxation of intermolecular motions in supercooled water and ice: A molecular dynamics study

*J. Chem. Phys.* **135**, 244511 (2011)

The role of the isothermal bulk modulus in the molecular dynamics of super-cooled liquids

*J. Chem. Phys.* **135**, 244508 (2011)

Experimental evidences for molecular origin of low-Q peak in neutron/x-ray scattering of 1-alkyl-3-methylimidazolium bis(trifluoromethanesulfonyl)amide ionic liquids

*J. Chem. Phys.* **135**, 244502 (2011)

A comparison of Coulombic interaction methods in non-equilibrium studies of heat transfer in water

*J. Chem. Phys.* **135**, 234111 (2011)

---

### Additional information on *J. Chem. Phys.*

Journal Homepage: <http://jcp.aip.org/>

Journal Information: [http://jcp.aip.org/about/about\\_the\\_journal](http://jcp.aip.org/about/about_the_journal)

Top downloads: [http://jcp.aip.org/features/most\\_downloaded](http://jcp.aip.org/features/most_downloaded)

Information for Authors: <http://jcp.aip.org/authors>

### ADVERTISEMENT

**AIP**Advances

*Submit Now*

Explore AIP's new  
open-access journal

- Article-level metrics now available
- Join the conversation! Rate & comment on articles

# Multiple time scale molecular dynamics for fluids with orientational degrees of freedom. I. Microcanonical ensemble

Igor P. Omelyan<sup>1,2,3,a)</sup> and Andriy Kovalenko<sup>1,2,b)</sup>

<sup>1</sup>National Institute for Nanotechnology, 11421 Saskatchewan Drive, Edmonton, Alberta, T6G 2M9, Canada

<sup>2</sup>Department of Mechanical Engineering, University of Alberta, Edmonton, Alberta, T6G 2G8, Canada

<sup>3</sup>Institute for Condensed Matter Physics, National Academy of Sciences of Ukraine, 1 Svientsitskii Street, UA-79011 Lviv, Ukraine

(Received 2 March 2011; accepted 22 August 2011; published online 20 September 2011)

We propose a new approach to eliminate the resonance instabilities inherent in multiple time step molecular dynamics simulations. The approach is developed within the microcanonical ensemble on the basis of an energy-constrained technique in the presence of orientational degrees of freedom. While the single and standard multiscale methods are restricted to small time steps of 5 and 8 fs, respectively, it is shown in simulations of water that the algorithms we have derived postpone the appearance of the instabilities to larger steps of about 16 fs. Such steps are close to the upper theoretical limit of 20 fs peculiar to the microcanonical ensemble and can be used without affecting static and dynamical properties. © 2011 American Institute of Physics. [doi:10.1063/1.3637035]

## I. INTRODUCTION

The coexistence of dynamical processes with vastly different time scales is a typical feature of many liquid systems in physics, chemistry, and biology.<sup>1–6</sup> The method of molecular dynamics (MD) remains one of the most fruitful approaches to study various properties in such fluids. However, the size of the time step in MD simulations is limited to rather small values to avoid numerical instabilities and achieve the desired accuracy of the calculations. Obviously, larger steps are more preferable because they give the possibility to reduce computational costs and get access to longer observation times. This, in turn, enables us to consider more complicated models of real liquids and reduce the statistical uncertainties to a minimum.

A variety of multiple time stepping (MTS) techniques has been devised over the last decades to improve the efficiency of MD simulations. They include the early intuitive schemes,<sup>7–13</sup> generalized Verlet integrator,<sup>14</sup> reversible reference system propagator algorithm (RESPA),<sup>15–17</sup> Langevin dynamics,<sup>18–20</sup> normal mode theories,<sup>21–24</sup> mollified impulse schemes,<sup>18,25–27</sup> canonical Nöse-Hoover-like<sup>28–30</sup> and isokinetic<sup>31</sup> thermostats, dynamical multiscale version,<sup>32</sup> isokinetic Nöse-Hoover chain approach,<sup>33,34</sup> as well as the processed MTS method.<sup>35</sup> In these techniques, each component of motion is integrated on its own physical time scale. Such an integration allows a significant speedup of the computations because then the costly long-range interactions can be sampled less frequently than the cheap strong forces.

It is now well established that the most adequate MTS integration can be carried out by decomposing the time evolution propagator into analytically solvable parts.<sup>15–17,28–35</sup> Within the microcanonical ensemble, this automatically provides the fulfilment of such important features of

Hamiltonian systems as the conservation of volume in phase space and time reversibility. Another advantage of the decomposition integrators, such as RESPA,<sup>15–17</sup> is their explicitness and simplicity. This is in contrast to the implicit normal mode schemes<sup>21,22</sup> which lead to iterative solutions and, moreover, require the calculation of cumbersome Hessian matrices. The same drawback is peculiar to the mollified integrators,<sup>18,25–27</sup> where the Hessians are involved to find averaged positions for the evaluation of weak interactions in quickly varying strong force fields. On the other hand, the dynamical multiscale version<sup>32</sup> is appropriate solely for simple models, such as harmonic oscillators, with a constant ratio of strong to weak potentials.

In RESPA, nevertheless, the size of the time step is restricted by resonance phenomena.<sup>36–40</sup> This means that a rapid energy growth occurs when the interval between the weak-force updates exceeds the half-period related to the fastest component of motion presented in the system. Within the Langevin-type algorithms,<sup>18–24,27</sup> the resonance instabilities are damped out by adding artificial friction and random forces to the equations of motions. But, this implies departure from the true microcanonical dynamics. In the canonical ensemble, the multiscale artifacts can be reduced by attaching extra phase-space variables corresponding to a thermostat.<sup>28–30</sup> Alternatively, the non-resonance equations can be derived in the isokinetic ensemble.<sup>31</sup> The instabilities can also be eliminated<sup>33,34</sup> by combining the canonical Nöse-Hoover method<sup>28</sup> with the isokinetic ensemble.<sup>31</sup> However, the isokinetic dynamics is fictitious and applicable only to study thermodynamic and position distribution functions. This is contrary to the microcanonical MD which can predict any given properties, including time correlation functions.

Surprisingly, almost all the existing MTS algorithms were designed to integrate translational motion exclusively. Usually, the molecular orientations are parameterized by Cartesian coordinates of atoms subject to holonomic constraints. However, this results in complicated iteration

<sup>a)</sup>Electronic mail: omelyan@icmp.lviv.ua.

<sup>b)</sup>Electronic mail: andriy.kovalenko@nrc-cnrc.gc.ca.

procedures such as Shake<sup>41</sup> or Rattle<sup>42</sup> to fix the intramolecular atomic distances. The problem of how to solve the equations of rotational motion in the microcanonical ensemble has been considered as well, but for single time step (STS) dynamics.<sup>43–52</sup> Only one paper<sup>53</sup> dealt, in fact, with the MTS propagation of orientational degrees of freedom. Using the rigid-body approximation for hydrogen containing segments in semiflexible molecules, a superiority of such an approach over the translational integrators has been demonstrated. The reason is that within the rotational equations of motion, the rigid structures of molecular segments are maintained intrinsically without involving any iterations. Unfortunately, this approach was limited to a canonical scheme with no emphasis on overcoming the MTS instabilities. Up to now, there were no MD algorithms that would enable reduction of these instabilities in the microcanonical ensemble.

In this paper, we propose and test a new MTS approach to suppress the resonance artifacts in the microcanonical ensemble. It is based on a novel energy-constrained technique combined with an extension of the recently introduced phase-space transforming method for translational motion<sup>35,52</sup> to the case when the orientational degrees of freedom are presented additionally. The MD simulations of ambient water demonstrate a clear advantage of the new approach, compared to the usual microcanonical MTS integrators.

The rest of the paper is organized as follows. The energy-constrained MTS algorithms are consistently derived in Sec. II. Their application to MD simulations of water and comparison with previously known integrators are described in Sec. III. Concluding remarks are highlighted in Sec. IV.

## II. THEORY

### A. Model of fluids and basic equations of motion

Consider a system of  $N$  molecules each of which is composed of  $M + M'$  interacting atoms. In the most general case, the first  $M = \sum_{k=1}^K M_k$  particles can form  $K$  rigid groups with  $M_k$  atoms for a given  $k = 1, 2, \dots, K$ . The other  $M'$  sites are flexibly connected between themselves and with the rigid-body atoms. The dynamical state of such a system in the laboratory frame at time  $t$  can be determined by the position  $\mathbf{r}_{ia}(t)$  and velocity  $\mathbf{v}_{ia}(t) = d\mathbf{r}_{ia}/dt$  of site  $a$  with mass  $m_a$  belonging to molecule  $i$ , where  $i = 1, 2, \dots, N$  and  $a = 1, 2, \dots, M + M'$ . In view of the rigidity, it is convenient to express the phase coordinates of  $M_k$  atoms in terms of the translational position  $\mathbf{R}_{ik}(t) = \mu_k^{-1} \sum_{a \in M_k} m_a \mathbf{r}_{ia}(t)$ , velocity  $\mathbf{V}_{ik}(t) = d\mathbf{R}_{ik}/dt$  of the center of mass  $\mu_k = \sum_{a \in M_k} m_a$  of the  $k$ -th group, its attitude matrix  $\mathbf{S}_{ik}(t)$ , and principal angular velocity  $\boldsymbol{\Omega}_{ik}(t)$  using the relations  $\mathbf{r}_{ia}(t) = \mathbf{R}_{ik}(t) + \mathbf{S}_{ik}^+(t)\boldsymbol{\delta}_{ak}$  and  $\mathbf{v}_{ia}(t) = \mathbf{V}_{ik}(t) + d\mathbf{S}_{ik}^+/dt\boldsymbol{\delta}_{ak}$ .

The elements of the attitude matrix  $\mathbf{S}_{ik}(t)$  represent the direction cosines between the principal axes of the molecular group and the laboratory frame, while  $\boldsymbol{\delta}_{ak}$  is the fixed position of site  $a$  with respect to the  $k$ th center of mass in the body-fixed frame. Note that  $\mathbf{S}_{ik}$  satisfies the orthonormality condition  $\mathbf{S}_{ik}\mathbf{S}_{ik}^+ = \mathbf{I}$ , where  $\mathbf{I}$  denotes the unit matrix and  $\mathbf{S}_{ik}^+$  is the result of transposition of  $\mathbf{S}_{ik}$ . This inherently maintains the rigid structures of molecular segments because the

action of  $\mathbf{S}_{ik}^+(t)$  on  $\boldsymbol{\delta}_{ak}$  does not change the interatomic distances within the molecule. The angular velocity is defined as  $d\mathbf{S}_{ik}/dt = \mathbf{W}(\boldsymbol{\Omega}_{ik})\mathbf{S}_{ik}$  with

$$\mathbf{W}(\boldsymbol{\Omega}) = \begin{pmatrix} 0 & \Omega_Z & -\Omega_Y \\ -\Omega_Z & 0 & \Omega_X \\ \Omega_Y & -\Omega_X & 0 \end{pmatrix} \quad (1)$$

being the skewsymmetric matrix related to the principal components  $(\Omega_X, \Omega_Y, \Omega_Z)$  of vector  $\boldsymbol{\Omega}$ .

The equations of translational and rotational motion can be written in the following compact form:

$$\frac{d\boldsymbol{\Gamma}}{dt} = L\boldsymbol{\Gamma}(t). \quad (2)$$

Here,

$$L = \sum_{i=1}^N \left( \sum_{k=1}^K \left[ \frac{\mathbf{P}_{ik}}{\mu_k} \cdot \frac{\partial}{\partial \mathbf{R}_{ik}} + \mathbf{W}(\mathbf{J}_k^{-1}\mathbf{S}_{ik}\mathbf{Q}_{ik})\mathbf{S}_{ik} \frac{\partial}{\partial \mathbf{S}_{ik}} + \mathbf{F}_{ik} \cdot \frac{\partial}{\partial \mathbf{P}_{ik}} + \boldsymbol{\Xi}_{ik} \cdot \frac{\partial}{\partial \mathbf{Q}_{ik}} \right] + \sum_{a=M+1}^{M+M'} \left[ \frac{\mathbf{p}_{ia}}{m_a} \cdot \frac{\partial}{\partial \mathbf{r}_{ia}} + \mathbf{f}_{ia}(\mathbf{r}, \mathbf{R}, \mathbf{S}) \cdot \frac{\partial}{\partial \mathbf{p}_{ia}} \right] \right) \quad (3)$$

is the Liouville operator of the system, while  $\boldsymbol{\Gamma}$  designates the set of all phase variables which includes  $K$  rigid groups  $\{\mathbf{R}, \mathbf{P}, \mathbf{S}, \mathbf{Q}\}$  with  $\mathbf{P}_{ik} = \mu_k \mathbf{V}_{ik}$  and  $\mathbf{Q}_{ik} = \mathbf{S}_{ik}^+ \mathbf{J}_k \boldsymbol{\Omega}_{ik}$  being the translational and angular momenta, respectively, in the laboratory frame, as well as  $M'$  individual coordinates and momenta  $\{\mathbf{r}, \mathbf{p}\}$ , where  $\mathbf{p}_{ia} = m_a \mathbf{v}_{ia}$ , belonging to flexibly connected atoms. Let us introduce the site-site potentials  $\varphi_{kl}$ ,  $\varphi_k$ , and  $\phi$  related correspondingly to the interactions between the rigid groups, between these groups and flexibly connected atoms, as well as between the latter atoms. Then, the force acting on the  $k$ th rigid group of molecule  $i$  due to the atomic interactions with the other groups and all flexibly jointed sites can be explicitly cast as  $\mathbf{F}_{ik} = \sum_{a \in M_k} \mathbf{F}_{ika}$ , where

$$\mathbf{F}_{ika} = - \sum_{j \neq i}^N \sum_{l=1}^K \sum_{b \in M_l} \hat{\mathbf{r}}_{ij}^{ab} \varphi'_{kl}(r_{ij}^{ab}) - \sum_{j=1}^N \sum_{b=M+1}^{M+M'} \hat{\mathbf{r}}_{ij}^{ab} \varphi'_k(r_{ij}^{ab}) \equiv \mathbf{F}_{ika}(\mathbf{R}, \mathbf{S}, \mathbf{r}), \quad (4)$$

while the forces exerting on such sites ( $a = M + 1, \dots, M + M'$ ) with respect to all other atoms are

$$\mathbf{f}_{ia} = - \sum_{j=1}^N \sum_{b=M+1}^{M+M'} \hat{\mathbf{r}}_{ij}^{ab} \phi'(r_{ij}^{ab}) \equiv \mathbf{f}_{ia}(\mathbf{R}, \mathbf{S}, \mathbf{r}). \quad (5)$$

In our notation  $\varphi'(r) \equiv d\varphi(r)/dr$  and  $\hat{\mathbf{r}}_{ij}^{ab} = (\mathbf{r}_{ia} - \mathbf{r}_{jb})/r_{ij}^{ab}$  with  $r_{ij}^{ab} = |\mathbf{r}_{ia} - \mathbf{r}_{jb}|$ . Having the atomic forces [Eq. (4)], the torque acted on the rigid molecular group with respect to its center of mass can be calculated as

$$\boldsymbol{\Xi}_{ik} = \sum_{a \in M_k} (\mathbf{r}_{ia} - \mathbf{R}_{ik}) \times \mathbf{F}_{ika} \equiv \boldsymbol{\Xi}_{ik}(\mathbf{R}, \mathbf{S}, \mathbf{r}). \quad (6)$$

It is worth pointing out that contrary to the intermolecular ( $i \neq j$ ) interactions  $\varphi_{kl}$ , the potentials  $\varphi_k$  and  $\phi$  consist of the intramolecular ( $i = j$ ) parts as well.

In view of the above, the total energy of the system can be expressed as

$$E = \sum_{i=1}^N \left( \sum_{k=1}^K \left[ \frac{\mu_k \mathbf{V}_{ik}^2}{2} + \sum_{\alpha}^{X,Y,Z} \frac{J_{k,\alpha} \Omega_{ik,\alpha}^2}{2} \right] + \sum_{a=M+1}^{M+M'} \frac{m_a \mathbf{v}_{ia}^2}{2} + \frac{1}{2} \sum_{j \neq i} \sum_{k,l=1}^K \sum_{a \in M_k} \sum_{b \in M_l} \varphi_{kl}(r_{ij}^{ab}) + \sum_{j=1}^N \sum_{k=1}^K \sum_{a \in M_k} \sum_{b=M+1}^{M+M'} \varphi_k(r_{ij}^{ab}) + \frac{1}{2} \sum_{j=1}^N \sum_{a,b=M+1}^{M+M'} \phi(r_{ij}^{ab}) \right), \quad (7)$$

where the first three terms relate to the kinetic part  $T(\mathbf{V}, \boldsymbol{\Omega}, \mathbf{v})$  and the rest three terms represent the full potential energy  $U(\mathbf{R}, \mathbf{S}, \mathbf{r})$ . Note that the term with  $a = b$  should be excluded, if  $j = i$  in the last sum of Eq. (7),  $J_{k,\alpha}$  denotes the diagonal elements of the time-independent matrix  $\mathbf{J}_k = \sum_{a \in M_k} m_a [(\delta_{ak} \cdot \delta_{ak}) \mathbf{I} - \delta_{ak} \delta_{ak}]$  of moments of inertia of the group along its principal axes, and  $\Omega_{ik,\alpha}$  are the components ( $\alpha = X, Y, Z$ ) of the principal angular velocity  $\boldsymbol{\Omega}_{ik} = \mathbf{J}_k^{-1} \mathbf{S}_{ik} \mathbf{Q}_{ik}$ .

The intermolecular parts ( $i \neq j$ ) of the atom-atom potentials  $\varphi_{kl}$ ,  $\varphi_k$ , and  $\phi$  can be presented<sup>34,54</sup> as the sum of the Lennard-Jones  $4\varepsilon_{ab}[(\sigma_{ab}/r_{ij}^{ab})^{12} - (\sigma_{ab}/r_{ij}^{ab})^6]$  and Coulombic  $q_a q_b / r_{ij}^{ab}$  interactions, where  $q_a$  is the charge of site  $a$ . The Lennard-Jones function includes the repulsion and van der Waals attraction. The intramolecular ( $i = j$ ) potential for a given pair  $ab$  of atoms can be modelled in  $\varphi_k$  and  $\phi$  by a harmonic oscillator  $u_l(r_{ii}^{ab} - l_0)^2/2$  or  $u_\theta(\theta_{ii}^{ab} - \theta_0)^2/2$ , where  $l_0$  or  $\theta_0$  are the equilibrium values of the bond length  $r_{ii}^{ab}$  or valence bend angle  $\theta_{ii}^{ab}$ . In addition, the torsional interactions  $u_n(1 + \cos(n\omega - \gamma))/2$  can also be included. They describe the periodic variation of energy due to bond rotations, where the low-order Fourier series in the dihedral angle  $\omega$  are employed with  $\gamma$  being the phase shift of the  $n$ -fold term. The parameters  $\varepsilon_{ab}$ ,  $\sigma_{ab}$ ,  $u_l$ ,  $u_\theta$ ,  $u_n$ ,  $l_0$ ,  $\theta_0$ , and  $\gamma$  can readily be found in the literature for each concrete molecular model of a fluid. For instance, in the case of water, the most popular among them are the rigid TIP3P/4P (Ref. 55) and SPC/E (Ref. 56) models, as well as their flexible TIP3P (Refs. 26 and 57) and SPC (Ref. 58) counterparts. For more complex molecules, (e.g., proteins and DNA), semiflexible models can be utilized. The corresponding parameters are available in AMBER (Ref. 59) and other force fields packages, such as OPLS,<sup>60</sup> CHARMM,<sup>61</sup> and GROMOS.<sup>62</sup> Note also that in a particular case when  $K = 0$  and  $M' = M$ , we reproduce a fully flexible model of fluids, while at  $K \neq 0$  and  $M' = 0$  we come to a mixture with  $K$  species each consisting of  $M_k$  rigid bodies.

If an initial configuration  $\boldsymbol{\Gamma}(0)$  is specified, the unique solution to the equations of motion [Eq. (2)] can be formally written as  $\boldsymbol{\Gamma}(t) = e^{Lt} \boldsymbol{\Gamma}(0)$ . However, the evolution operator  $e^{Lt}$  cannot be evaluated exactly for any time  $t$ , and the only way is to approximate it using numerical methods.

## B. Standard MTS splitting technique

In the splitting approach, the Liouville operator  $L = A + B$  is decomposed into the kinetic  $A$  and potential  $B$  parts. In view of Eq. (3), the explicit expressions for them in our case are  $A = \mathbf{p} \cdot \partial/\partial \mathbf{r} + \mathbf{P} \cdot \partial/\partial \mathbf{R} + \mathbf{W}(\mathbf{J}^{-1} \mathbf{S} \mathbf{Q}) \mathbf{S} \partial/\partial \mathbf{S}$  and  $B = \mathbf{f} \cdot \partial/\partial \mathbf{p} + \mathbf{F} \cdot \partial/\partial \mathbf{P} + \boldsymbol{\Xi} \cdot \partial/\partial \mathbf{Q}$ . Here, all the indices have been omitted to simplify notation. For the same reason, the first terms in  $A$  and  $B$  can be omitted as well since they are quite similar to the second terms (with formal replacements of capital and small letters). Moreover, we will assume that there are only two scales of time (the extension to an arbitrary number of time scales is trivial).

Proceeding now in the spirit of the standard MTS schemes,<sup>15,16</sup> the total force  $\mathbf{F} = \mathbf{F}_s + \mathbf{F}_w$  and torque  $\boldsymbol{\Xi} = \boldsymbol{\Xi}_s + \boldsymbol{\Xi}_w$  are split up into the strong  $\mathbf{F}_s$  and  $\boldsymbol{\Xi}_s$  as well as the weak  $\mathbf{F}_w$  and  $\boldsymbol{\Xi}_w$  components related to the short-ranged  $\varphi_s$  and long-ranged  $\varphi_w$  interactions, respectively, with  $\varphi = \varphi_s + \varphi_w$ . This will result in further decomposition of the potential part as  $B = B_s + B_w$  with  $B_{s,w} = \mathbf{F}_{s,w} \cdot \partial/\partial \mathbf{P} + \boldsymbol{\Xi}_{s,w} \cdot \partial/\partial \mathbf{Q}$ , where  $B_s$  and  $B_w$  are responsible correspondingly for the fast and slow processes in the system. Then, generalizing the Trotter formula,<sup>63</sup> the time evolution propagator  $e^{Lh}$  can be factorized as  $e^{[(A+B_s+B_w)+\mathcal{E}(h^2)]h} = e^{B_w \frac{h}{2}} [e^{B_s \frac{h}{2n}} e^{A \frac{h}{n}} e^{B_s \frac{h}{2n}}]^n e^{B_w \frac{h}{2}}$ , where  $h$  is the size of the outer time step,  $n$  is the number of inner loops, and  $\mathcal{E}(h^2)$  is the local second-order error function. For any time  $t$ , the solution can be presented in the form

$$\boldsymbol{\Gamma}(t) = [e^{B_w \frac{h}{2}} [e^{B_s \frac{h}{2n}} e^{A \frac{h}{n}} e^{B_s \frac{h}{2n}}]^n e^{B_w \frac{h}{2}}]^l \boldsymbol{\Gamma}(0) + \mathcal{O}(h^2), \quad (8)$$

where  $\mathcal{O}(h^2) \sim l \mathcal{E}(h^2) h$  is the global error and  $l = t/h$  is the total number of steps. In the absence of orientational degrees of freedom, one reproduces from Eq. (8) at  $n = 1$  the well-known Verlet integrator,<sup>64,65</sup> while for  $n > 1$  we come to the second-order RESPA scheme.<sup>15,16</sup> In the latter case, the strong-force component is integrated with a smaller time step of  $h/n$  than that of  $h$  related to the weak-interaction contribution. This speeds up the calculations because then the expensive long-ranged forces will not be recalculated so frequently.

The main advantage of the splitting approach [Eq. (8)] is that the action of the exponentials  $e^{Ah/n}$ ,  $e^{B_s h/(2n)}$ , and  $e^{B_w h/2}$  on a phase space point  $\boldsymbol{\Gamma}$  can be given analytically. Indeed<sup>52</sup>

$$e^{A \frac{h}{n}} \{\mathbf{R}, \mathbf{P}, \mathbf{S}, \mathbf{Q}\} = \{\mathbf{R} + \mu^{-1} \mathbf{P} \frac{h}{n}, \mathbf{P}, \boldsymbol{\Psi}(\mathbf{Q}, \frac{h}{n}) \mathbf{S}, \mathbf{Q}\},$$

$$e^{B_s \frac{h}{2n}} \{\mathbf{R}, \mathbf{P}, \mathbf{S}, \mathbf{Q}\} = \{\mathbf{R}, \mathbf{P} + \mathbf{F}_s \frac{h}{2n}, \mathbf{S}, \mathbf{Q} + \boldsymbol{\Xi}_s \frac{h}{2n}\}, \quad (9)$$

$$e^{B_w \frac{h}{2}} \{\mathbf{R}, \mathbf{P}, \mathbf{S}, \mathbf{Q}\} = \{\mathbf{R}, \mathbf{P} + \mathbf{F}_w \frac{h}{2}, \mathbf{S}, \mathbf{Q} + \boldsymbol{\Xi}_w \frac{h}{2}\},$$

where the displacement of  $\mathbf{R}$  corresponds to free translational motion (i.e.,  $\mathbf{P}$  is constant), while the shifts in  $\mathbf{P}$  and  $\mathbf{Q}$  relate to uniformly accelerated motion in instantaneous force-torque fields at given  $\mathbf{R}$  and  $\mathbf{S}$ . The matrix  $\boldsymbol{\Psi}(\mathbf{Q}, \frac{h}{n})$  exactly<sup>66</sup> propagates  $\mathbf{S}$  over time  $h/n$  according to the free rotational dynamics ( $\mathbf{Q}$  remains constant). Alternatively,<sup>52</sup>  $\boldsymbol{\Psi}(\mathbf{Q}, \Delta t)$  can be replaced by its decomposition counterpart  $\boldsymbol{\Psi}_2(\Delta t) = \Theta(\Omega_X, \frac{\Delta t}{2}) \Theta(\Omega_Y, \frac{\Delta t}{2}) \Theta(\Omega_Z, \Delta t) \Theta(\Omega_Y, \frac{\Delta t}{2}) \Theta(\Omega_X, \frac{\Delta t}{2})$  of the second-order at  $\Delta t = h/n$ , where  $\Theta(\Omega_\alpha, \Delta t) = \exp[\mathbf{W}(\Omega_\alpha) \Delta t]$  is the matrix of rotation on angle  $\Omega_\alpha \Delta t$  around axis  $\alpha$  at constant component  $\Omega_\alpha$  of  $\boldsymbol{\Omega} = \mathbf{J}^{-1} \mathbf{S} \mathbf{Q}$ .

As pointed out in the Introduction, the RESPA integration exhibits the resonance instability already at relatively small values of  $h$ , even through  $n \gg 1$ . We will now consider the question of how to suppress such instabilities in the microcanonical ensemble.

### C. Advanced energy-targeted approach

The main idea to efficiently reduce the MTS instabilities within the microcanonical ( $NVE$ ) ensemble lies in the following. It is well known that the total energy of an isolated system remains constant, i.e.,  $E(t) = E_0 = \text{const.}$ , provided the equations of motion are solved exactly. In practice, however, we deal with an approximate integration, so that the total energy will not be conserved precisely. For this reason, it is quite natural to treat the desired equality  $E(t) = E_0$ , where  $E_0 = E(0)$ , as a constraint imposed on the equations of motion in the  $NVE$  ensemble. The fact that the coordinates and velocities are connected by this constraint leads, in general, to the necessity of the introduction of constraint forces  $\mathbf{F}_\lambda$  and torques  $\mathbf{\Xi}_\lambda$ . Because the energy constraint is non-holonomic, they can be written<sup>67</sup> in the form  $\mathbf{F}_\lambda = -\lambda \partial E / \partial \mathbf{V} = -\lambda \mu \mathbf{V}$  and  $\mathbf{\Xi}_\lambda = -\lambda \partial E / \partial \mathbf{\Omega} = -\lambda \mathbf{J} \mathbf{\Omega}$ . Note that the Lagrange multiplier  $\lambda$  is equal to zero in the hypothetical case of exactly produced phase trajectories (then the energy constraint will be satisfied automatically). In view of this, the above constraint forces and torques are virtual. They are aimed only at the compensation of uncertainties caused by the approximate character of the numerical integration.

In the presence of the energy constraint, the time propagation [Eq. (8)] modifies to

$$\Gamma(t) = [e^{B_\lambda \frac{h}{2}} e^{B_w \frac{h}{2}} [e^{B_s \frac{h}{2n}} e^{A \frac{h}{n}} e^{B_s \frac{h}{2n}}]^n e^{B_w \frac{h}{2}} e^{B_\lambda \frac{h}{2}}]^l \Gamma(0), \quad (10)$$

where  $B_\lambda = \mu^{-1} \mathbf{F}_\lambda \cdot \partial / \partial \mathbf{V} + \mathbf{J}^{-1} \mathbf{\Xi}_\lambda \cdot \partial / \partial \mathbf{\Omega}$ . The action of the exponential  $e^{B_\lambda \frac{h}{2}}$  on  $\mathbf{V}$  and  $\mathbf{\Omega}$  results in  $e^{B_\lambda \frac{h}{2}} \{\mathbf{V}, \mathbf{\Omega}\} = \exp(-\lambda h/2) \{\mathbf{V}, \mathbf{\Omega}\}$  or in the momentum representation

$$e^{B_\lambda \frac{h}{2}} \{\mathbf{P}, \mathbf{Q}\} = \exp(-\lambda h/2) \{\mathbf{P}, \mathbf{Q}\}. \quad (11)$$

After each  $l = 1, 2, \dots, t/h$ , the current value of the Lagrange multiplier  $\lambda$  could be found by satisfying exactly the constraint  $E_l = E_0$ , where  $E_l = E(lh)$  is the total energy of the system at time  $lh$ . Then, one obtains  $\lambda h/2 = -\ln(1 + \delta E/2)$ , where  $\delta E = [1 - (E_l - E_0)/T_l]^{1/2} - 1$  at  $T_l = T(lh)$  is the instantaneous kinetic energy of the system. A much more gentle way is to restore only a small fraction  $\xi \ll 1$  of the energy deviation  $E_l - E_0$  when constructing the virtual viscosity  $\lambda$ . This yields  $\lambda h/2 = -\ln(1 + \delta E_\xi/2)$ , where  $\delta E_\xi = [1 - \xi(E_l - E_0)/T_l]^{1/2} - 1$ . Taking into account that  $(E_l - E_0)/T_l \sim \mathcal{O}(h^2)$ , one finds  $\lambda h = \frac{1}{2} \xi (E_l - E_0)/T_l + \mathcal{O}(h^4)$ .

The parameter  $\xi \ll 1$  determines the strength of coupling of the system with an energetic bath. It can be defined as the ratio  $\xi = h/\tau \ll 1$ , where  $\tau$  is the relaxation time characterizing the bath. At  $\tau \rightarrow \infty$ , we come to usual (unconstrained) microcanonical simulations. Note that formally putting  $\tau = h$  leads to the standard velocity rescaling scheme. Such a scheme must not be used because of possible numerical artifacts, such as violation of the equipartition

theorem.<sup>68,69</sup> In order to avoid any side effects, the quantity  $\tau$  should be large enough with respect to a characteristic time interval related to the correlation functions under investigation. On the other hand, it should be finite in order to properly provide the conservation of the total energy. It is interesting to remark that the proposed energy-targeted approach looks somewhat similar to the Berendsen thermostat.<sup>70,71</sup> However, a crucial difference is that now our aim is to conserve the total energy instead of temperature. The latter together with the potential energy fluctuates according to the true microcanonical distribution, because the unphysical energy deviations are reduced to a minimum. This is contrary to the Berendsen thermostat, where the velocity distribution does not necessarily satisfy the properties of the canonical ensemble.<sup>3,71,72</sup>

The precision of the energy-targeted scheme can be improved further by using a so-called processed technique.<sup>35,52</sup> It is based on canonical-like transformations of phase space for reducing the energy fluctuations in the microcanonical ensemble. For the case of the MTS integration with orientational degrees of freedom, such transformations of the real phase space  $\Gamma = \{\mathbf{R}, \mathbf{P}, \mathbf{S}, \mathbf{Q}\}$  will read

$$\mathfrak{T} \Gamma = \tilde{\Gamma} = \{\tilde{\mathbf{R}}, \tilde{\mathbf{P}}, \tilde{\mathbf{S}}, \tilde{\mathbf{Q}}\}. \quad (12)$$

Taking into account the structure of the second-order error function  $\mathcal{E}(h^2)$  in Eq. (8), one obtains

$$\begin{aligned} \tilde{\mathbf{R}} &= \mathbf{R} - h^2 \mu^{-1} [\alpha_s^t \mathbf{F}_s(\tilde{\mathbf{R}}, \tilde{\mathbf{S}})/n^2 + \alpha_w^t \mathbf{F}_w(\tilde{\mathbf{R}}, \tilde{\mathbf{S}})], \\ \tilde{\mathbf{P}} &= \mathbf{P} + h^2 [\beta_s^t \dot{\mathbf{F}}_s(\tilde{\Gamma})/n^2 + \beta_w^t \dot{\mathbf{F}}_w(\tilde{\Gamma})], \\ \tilde{\mathbf{S}} &= \Theta(-\mathbf{J}^{-1} \tilde{\mathbf{S}} [\alpha_s^t \mathbf{\Xi}_s(\tilde{\mathbf{R}}, \tilde{\mathbf{S}})/n^2 + \alpha_w^t \mathbf{\Xi}_w(\tilde{\mathbf{R}}, \tilde{\mathbf{S}})], h^2) \mathbf{S}, \\ \tilde{\mathbf{Q}} &= \mathbf{Q} + [\beta_s^t \dot{\mathbf{\Xi}}_s(\tilde{\Gamma})/n^2 + \beta_w^t \dot{\mathbf{\Xi}}_w(\tilde{\Gamma})] h^2, \end{aligned} \quad (13)$$

where  $\alpha_{s,w}^{t,r}$  and  $\beta_{s,w}^{t,r}$  are the parameters which will be defined later.

In view of Eqs. (10) and (12), the solution to the equations of motion can be cast in the form

$$\begin{aligned} \Gamma(t) &= [\mathfrak{T}^{-1} e^{B_\lambda \frac{h}{2}} e^{B_w \frac{h}{2}} [e^{B_s \frac{h}{2n}} e^{A \frac{h}{n}} e^{B_s \frac{h}{2n}}]^n e^{B_w \frac{h}{2}} e^{B_\lambda \frac{h}{2}} \mathfrak{T}]^l \\ &\quad \times \Gamma(0) + \mathcal{O}(h^2), \end{aligned} \quad (14)$$

where the single exponentials act now in the transformed phase space on  $\tilde{\mathbf{R}}$  and  $\tilde{\mathbf{P}}$  as well as  $\tilde{\mathbf{S}}$  and  $\tilde{\mathbf{Q}}$  using the same rules as for  $\mathbf{R}, \mathbf{P}, \mathbf{S}$ , and  $\mathbf{Q}$  [see Eqs. (9) and (11)]. Therefore, during the processed propagation [Eq. (14)], the operator  $\mathfrak{T}$  first transforms the original phase point  $\Gamma$  to the time-step dependent pseudo-dynamical variables  $\tilde{\Gamma}$  [see Eq. (12)] according to Eq. (13). Further, the new variables are updated using Eqs. (9) and (11). The solution in the real phase space  $\Gamma$  is then decoded from  $\tilde{\Gamma}$  applying the inverse transformation  $\mathfrak{T}^{-1} \tilde{\Gamma}$ . Finally, the current total energy  $E_l$  is evaluated in the original space  $(\mathbf{R}, \mathbf{P}, \mathbf{S}, \mathbf{Q})$  to calculate the new value  $\lambda = (1/2\tau)(E_l - E_0)/K_l$  of the virtual friction coefficient. The procedure is repeated  $l = t/h$  times to obtain the phase point  $\Gamma(t)$  at any  $t$ . Note that in order to reduce the computational overhead on the calculation of  $E_l$ , the friction coefficient can be updated not so frequently but after a few ( $\kappa \sim 5$ ) outer time steps.

It can be shown after cumbersome algebra using an error function analysis that the processed algorithm [Eq. (14)],

even at the absence of virtual forces ( $\lambda = 0$ ), exactly conserves the energy corresponding to a nearby Hamiltonian  $E + \Delta E + \mathcal{O}(h^4)$ , where the deviation from  $E$  [Eq. (7)] is  $\Delta E = \Delta E_t + \Delta E_r$ . For instance, the translational motion contribution has the form<sup>35</sup>

$$\begin{aligned} \Delta E_t = & \frac{h^2}{\mu} \left[ \left( \frac{\alpha_s^t - 1/24}{n^2} \mathbf{F}_s \cdot \mathbf{F}_s + (\alpha_w^t - 1/24) \mathbf{F}_w \cdot \mathbf{F}_w \right) \right. \\ & + \left( \frac{\alpha_s^t}{n^2} + \alpha_w^t - 1/12 \right) \mathbf{F}_s \cdot \mathbf{F}_w \\ & \left. + \left( \frac{\beta_s^t - 1/12}{n^2} \dot{\mathbf{F}}_s + (\beta_w^t - 1/12) \dot{\mathbf{F}}_w \right) \cdot \mathbf{P} \right]. \quad (15) \end{aligned}$$

The expression for the rotational part  $\Delta E_r$  is similar to Eq. (15) with formal replacements of  $\mathbf{F}$  by  $\mathbf{\Xi}$  and  $\mathbf{P}$  by  $\mathbf{Q}$ .

Thus, the parameters  $\alpha_{s,w}^{t,r}$  and  $\beta_{s,w}^{t,r}$  should be chosen in such a way as to provide a minimum for the norm  $|\Delta E|$  of  $\Delta E$ . The obvious choice for  $\beta$ -parameters is  $\beta_s^{t,r} = \beta_w^{t,r} = 1/12$ ; since then, the terms with the time derivatives are canceled out completely. The  $\alpha$ -parameters should minimize the remaining terms of the norm  $|\Delta E|$ . The latter depends on the ratios  $\gamma_t = |\mathbf{F}_s|/|\mathbf{F}_w|$  and  $\gamma_r = |\mathbf{\Xi}_s|/|\mathbf{\Xi}_w|$  of the norms  $|\mathbf{F}_s|$  and  $|\mathbf{F}_w|$  or  $|\mathbf{\Xi}_s|$  and  $|\mathbf{\Xi}_w|$ . These norms represent in fact the root-mean-square values of the short- and long-ranged forces or torques acting on the molecules, i.e.,  $|\mathbf{F}_s| = \langle \mathbf{F}_s \cdot \mathbf{F}_s \rangle^{1/2}$  and  $|\mathbf{F}_w| = \langle \mathbf{F}_w \cdot \mathbf{F}_w \rangle^{1/2}$  or  $|\mathbf{\Xi}_s| = \langle \mathbf{\Xi}_s \cdot \mathbf{\Xi}_s \rangle^{1/2}$  and  $|\mathbf{\Xi}_w| = \langle \mathbf{\Xi}_w \cdot \mathbf{\Xi}_w \rangle^{1/2}$ , where  $\langle \dots \rangle$  denotes statistical averaging. The parameters  $\alpha_{s,w}^{t,r}$  are then found from the extremum conditions  $\partial|\Delta E|/\partial\alpha_s = 0$  and  $\partial|\Delta E|/\partial\alpha_w = 0$ . This yields

$$\alpha_s^{t,r} = \frac{1}{24} \frac{\gamma^2 + \gamma^4 + n^2}{1 + \gamma^2 + \gamma^4}, \quad \alpha_w^{t,r} = \frac{1 + \gamma^2 + \gamma^4(2 - 1/n^2)}{24(1 + \gamma^2 + \gamma^4)}, \quad (16)$$

where  $\gamma \equiv \gamma_t$  or  $\gamma_r$ . The best choice for the MTS number  $n$  is to provide the integration of each component of motion on its own time scale with nearly the same (second-order) accuracy, so that  $n \sim \gamma^{1/2}$ . The additional minimization of  $|\Delta E_r|$  (and thus  $|\Delta E|$ ) can be achieved by adding extra ( $\tilde{\mathbf{S}}\tilde{\mathbf{Q}}$ -like) terms to the last line of Eq. (13) when transforming (by  $\mathfrak{T}^{-1}\tilde{\mathbf{F}}$ ) the angular momenta, namely,

$$\begin{aligned} \mathbf{Q} = & \tilde{\mathbf{Q}} - (\mathbf{I} + \frac{1}{4}\tilde{\mathbf{S}}^+[\mathbf{J}\mathbf{W}(\mathbf{J}^{-1}\tilde{\mathbf{S}}\tilde{\mathbf{Q}})\mathbf{J}^{-1} - \mathbf{W}(\mathbf{J}^{-1}\tilde{\mathbf{S}}\tilde{\mathbf{Q}}) \\ & - \mathbf{W}(\tilde{\mathbf{S}}\tilde{\mathbf{Q}})\mathbf{J}^{-1}]\tilde{\mathbf{S}})[\beta_s^r \dot{\mathbf{\Xi}}_s(\tilde{\mathbf{F}})/n^2 + \beta_w^r \dot{\mathbf{\Xi}}_w(\tilde{\mathbf{F}})]h^2. \quad (17) \end{aligned}$$

The RESPA appears to be a particular case of Eq. (14), when  $\alpha_{s,w} = \beta_{s,w} = \lambda = 0$  and the orientational degrees of freedom are absent. For  $\alpha_{s,w} = \beta_{s,w} = 0$  and  $\lambda \neq 0$ , we come to Eq. (10) which will be referred to as the energy-targeted rotational-motion RESPA (ERESPA) scheme. At  $\lambda = 0$  with  $\beta_{s,w} = 1/12$  and  $\alpha_{s,w} \neq 0$  [Eq. (16)], the integration given by Eq. (14) will be named by the processed (optimized) MTS (OMTS) algorithm. Its energy-constrained ( $\lambda \neq 0$ ) counterpart will be abbreviated by EOMTS.

Because of  $\mathfrak{T}^{-1}\mathfrak{T} = \mathbf{I}$ , the real variables  $\mathbf{\Gamma}$  are not involved into the EOMTS integration and are reproduced by  $\mathbf{\Gamma} = \mathfrak{T}^{-1}\tilde{\mathbf{F}}$  whenever measurement is necessary. Then, the

time derivatives  $\dot{\mathbf{F}}_{s,w}(\tilde{\mathbf{F}})$  and  $\dot{\mathbf{\Xi}}_{s,w}(\tilde{\mathbf{F}})$  in  $\mathfrak{T}^{-1}$  can be evaluated at  $t$  using the interpolation with  $h_s = h/n$  and  $h_w = h$ , where  $\mathbf{G} \equiv \mathbf{F}$  or  $\mathbf{\Xi}$ . For  $\dot{\mathbf{G}}_s(\tilde{\mathbf{F}})$ , this interpolation implies that  $\mathbf{G}_s(t + qh/n) = \mathbf{G}_s(\tilde{\mathbf{R}}_q, \tilde{\mathbf{S}}_q)$ , where  $\tilde{\mathbf{R}}_q$  and  $\tilde{\mathbf{S}}_q$  are the consecutive ( $q = -1, 0, 1$ ) values of  $\tilde{\mathbf{R}}$  and  $\tilde{\mathbf{S}}$  obtained by the inner loop displacements within the two ( $\mp$ ) neighboring outer steps with  $\tilde{\mathbf{R}}_0 = \tilde{\mathbf{R}}(t)$  and  $\tilde{\mathbf{S}}_0 = \tilde{\mathbf{S}}(t)$  ( $n \geq 2$ ). For  $\mathbf{G}_w(\tilde{\mathbf{F}})$ , the interpolation is possible since  $\tilde{\mathbf{F}}$  is propagated independently of  $\mathbf{\Gamma}$ . Thus,  $\mathbf{\Gamma}(t)$  can be reproduced from the set  $\tilde{\mathbf{F}}(t + qh)$  with the one-step retardation, when the pseudo-phase variables were already propagated to  $\tilde{\mathbf{F}}(t + h)$  and the values  $\mathbf{G}_w(t + qh) = \mathbf{G}_w(\tilde{\mathbf{R}}(t + qh))$  are known from the integration. Such a postprocessing avoids calculation of any additional forces and torques.

### III. MD SIMULATIONS

The algorithms derived in Sec. II will now be examined in actual MD simulations. The system considered was the TIP4P model of water<sup>55</sup> with one ( $K = 1$ ) rigid group containing  $M = 4$  interaction sites per molecule and no ( $M' = 0$ ) flexibly jointed atoms. We placed  $N = 512$  molecules in a cubic box of volume  $V = L^3$  to which the periodic boundary conditions are applied. The simulations were carried out at ambient density  $N/V = 1$  g/cm<sup>3</sup> and temperature  $\mathcal{T} = 293$  K. The Coulombic interactions were handled using the Ewald summation technique<sup>73</sup> at  $R_c = L/2 = 12.417$  Å with  $\kappa_{\max} = 8$  and  $\zeta L = 7.251$ . Here,  $R_c$  and  $\kappa_{\max}$  are the cutoff radii in the real and reciprocal space, respectively, while  $\zeta$  denotes the screening parameter. In such a way, the total intermolecular forces  $\mathbf{F}$  were found.

The strong (s) component  $\mathbf{F}_s$  of  $\mathbf{F}$  has been determined in the spirit of the near/far distance based approach<sup>16,74-77</sup> with the help of Eq. (4) by replacing  $\phi'(r)$  with  $w(r)\phi'(r)$ . The switching function was chosen in the form of the cubic spline<sup>77</sup>  $w(r) = 1 - (10 - 15\eta + 6\eta^2)\eta^3$  with  $\eta = 1 + (r - r_c)/(r_0 - r_c)$  to smoothly change its value from 1 to 0 when increasing the interatomic distance  $r$  from  $r_0$  to  $r_c \leq L/2$ . The weak (w) component  $\mathbf{F}_w$  of the intermolecular forces  $\mathbf{F} = \mathbf{F}_s + \mathbf{F}_w$  was then found by extracting  $\mathbf{F}_s$  from  $\mathbf{F}$ , i.e.,  $\mathbf{F}_w = \mathbf{F} - \mathbf{F}_s$ . Such an approach appears to be more efficient than the straightforward real/reciprocal splitting of Coulombic interactions.<sup>75,77</sup> Having  $\mathbf{F}_s$  and  $\mathbf{F}_w$ , the intermolecular torques  $\mathbf{\Xi} = \mathbf{\Xi}_s + \mathbf{\Xi}_w$  were decomposed into the strong  $\mathbf{\Xi}_s$  and weak  $\mathbf{\Xi}_w$  components exploiting Eq. (6) with formal replacement of  $\mathbf{F}$  by  $\mathbf{F}_s$  or  $\mathbf{F}_w$ . Note that  $w(r) = 1$  for  $r \leq r_0$  and  $w(r) = 0$ , if  $r \geq r_c$ . The cutoff radius of the short-ranged interaction was  $r_c = 9$  Å  $< R_c = L/2$  at the switching-on parameter  $r_0 = 3$  Å. For this choice, the ratios  $\gamma_t = |\mathbf{F}_s|/|\mathbf{F}_w|$  and  $\gamma_r = |\mathbf{\Xi}_s|/|\mathbf{\Xi}_w| = |\mathbf{G}_s|/|\mathbf{G}_w|$  of the strong to weak interactions were equal to  $\gamma_t \approx 30$  and  $\gamma_r \approx 16$ , respectively.

The equations of motion were solved using the processed algorithm OMTS, its energy-targeted extension EOMTS, the energy-constrained version ERESPA, the single time step Verlet-like integrator, and the original RESPA scheme. All these algorithms are comprehensively described in Sec. II C [see Eqs. (10)–(17)]. Note that the first three of them are new. A lot of stepsizes  $h$  lying in the interval  $h \in [0.1, 20]$  fs were

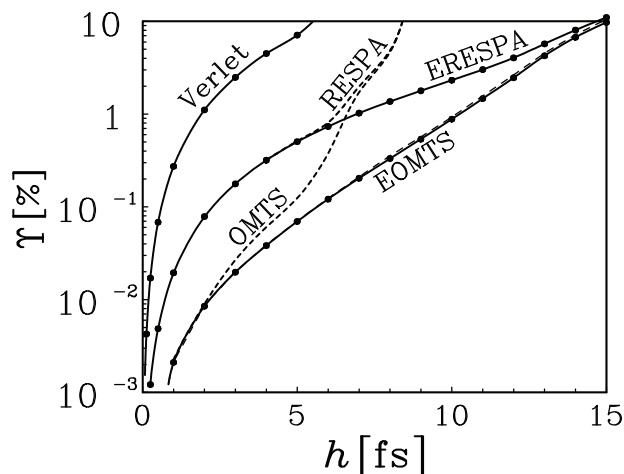


FIG. 1. The averaged relative total energy fluctuations  $\Upsilon$  in the microcanonical MD simulations of ambient TIP4P water corresponding to different algorithms with various time steps  $h$ .

employed for each integrator. For the constrained schemes EOMTS and ERESPA, the relaxation time of the virtual energetic bath was taken to be  $\tau = 200$  fs. The MTS parameter was equal to  $n = 5 \approx \max(\gamma_t, \gamma_r)^{1/2}$ . All MD runs were started from an identical well equilibrated initial configuration  $\rho(0)$ . Extremely long duration simulations with the total number  $l = t/h = 10^6$  of steps have been performed to analyze numerical stability of the time propagation. The accuracy of the integration was measured in terms of the ratio  $\Upsilon = [(\langle E^2 \rangle / \langle E \rangle^2 - 1) / (\langle U^2 \rangle / \langle U \rangle^2 - 1)]^{1/2}$  of the total energy fluctuations to the fluctuations of the potential energy  $U$ . We mention that in the microcanonical ensemble, the full energy is a constant of motion,  $E = \text{const.}$ , leading to  $\Upsilon \equiv 0$ . In approximate MD simulations, however, the total energy is not

conserved exactly, so that smaller values of  $\Upsilon \neq 0$  indicate a better precision of the integration.

The dependency of the averaged relative total energy fluctuations  $\Upsilon$  on the size of the outer time step  $h$ , obtained in the MD simulations of the TIP4P model of water at the fixed length  $t/h = 10^6$  with the help of the EOMTS algorithm, is shown in Fig. 1. For comparison, the corresponding functions  $\Upsilon(h)$  related to the Verlet, RESPA, ERESPA, and OMTS integrators are also included. As can be seen, the STS Verlet scheme becomes unstable already at  $h > h_{\text{STS}} \approx 5$  fs, where it is inapplicable because of too large energy fluctuations ( $\Upsilon \gtrsim 10\%$ ). More efficient simulations are observed within the RESPA and OMTS integrators, where the maximum allowable size of the outer step increases to  $h \sim 8$  fs. At the same time, in the usual region  $h \lesssim 5$  fs, the OMTS scheme provides much more precise integration than RESPA. However, the best result is achieved within the energy-targeted ERESPA and EOMTS algorithms. They allow us to use considerably larger outer time steps up to values of  $h \sim 15$  fs. Such values are close to the upper theoretical limit  $h_{\text{MTS}} = \min(\gamma_t, \gamma_r)^{1/2} h_{\text{STS}} \approx 20$  fs inherent in the microcanonical MD simulations. Moreover, at moderate and small time steps of  $h \lesssim 10$  fs, the EOMTS algorithm is able to significantly decrease the unphysical energy fluctuations, compared to the ERESPA scheme. For  $h \lesssim 5$  fs, the processed algorithm OMTS and its energy-targeted version EOMTS lead practically to the same energy conservation.

Samples of the normalized deviations  $\delta E(t) = (E(t) - E_0)/E_0$  of the total energy  $E$ , obtained at the most characteristic time steps within the standard RESPA and processed OMTS algorithms as well as within their energy-targeted counterparts ERESPA and EOMTS, are plotted in Fig. 2 versus the length  $t/h$  of the simulations. We see that the

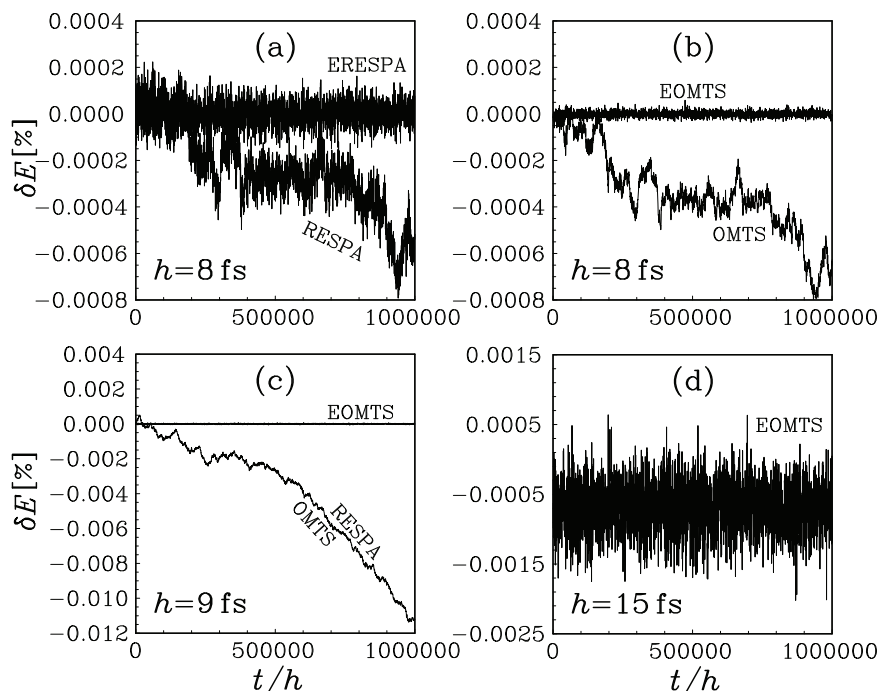


FIG. 2. The relative instantaneous values  $\delta E$  of the total energy  $E$  versus the length  $t$  of the microcanonical MD simulations carried out for the TIP4P water with different algorithms at a few characteristic time steps  $h$ .

ERESPA and EOMTS integrators demonstrate excellent stability properties. For instance, the EOMTS instantaneous energy  $E(t)$  stays near its initial level  $E_0$ , even after  $t/h = 10^6$  steps with large sizes of  $h = 15$  fs. This is contrary to the non-constrained RESPA and OMTS schemes which beginning from relatively small values  $h = 8$  fs clearly exhibit the instability due to the MTS resonance. The influence of this resonance on the RESPA and OMTS results increases rapidly with increasing  $h$  so that already at  $h > 8$  fs, such schemes cannot be used. On the other hand, the resonance instability is efficiently eliminated by the proposed ERESPA and EOMTS algorithms up to time steps of order  $h \sim 15$  fs.

It is worth emphasizing that as in the non-constrained integrators, the full energy  $E$  within the ERESPA and EOMTS algorithms is not conserved exactly. Instead, it fluctuates around the initial value  $E_0$  almost with the same local magnitude as in the RESPA and OMTS integrators (see Fig. 2). This is because a very small portion  $(1/2)h/\tau \ll 1$  of the deviation  $(E(t) - E_0)/T$  was used to build the constrained forces and torques. Since the relaxation time of the energetic bath was chosen to be  $\tau = 200$  fs, the fraction  $(1/2)h/\tau$  does not exceed a value of 3.75%, even at  $h \sim 15$  fs. At such a choice of  $\tau$ , the virtual forces  $\mathbf{F}_\lambda$  and torques  $\mathbf{\Xi}_\lambda$  appear to be negligibly small not only with respect to the original strong (short-ranged) interactions, but also with respect to the weak (long-ranged) forces and torques as well. In particular, the ratios of strengths  $|\mathbf{F}_\lambda|/|\mathbf{F}_w|$  and  $|\mathbf{\Xi}_\lambda|/|\mathbf{\Xi}_w|$  were 1% at  $h = 15$  fs or less for smaller time steps. Thus, Eq. (11) corresponds to a very mild rescaling of translational and angular velocities [which is applied in Eq. (10) after each outer time step]. Despite the smallness of the virtual interactions, they have allowed us to achieve an amazing stabilizing effect on the conservation of the total energy during the long-term microcanonical MTS simulations.

In order to ensure that the new algorithms indeed postpone the appearance of the MTS resonances to larger time steps without any masking effects, we have performed additional measurements concerning some other characteristic observable quantities. They include the oxygen-oxygen (OO), hydrogen-hydrogen (HH), and oxygen-hydrogen (OH) radial distributions  $g_{OO}(r)$ ,  $g_{HH}(r)$ , and  $g_{OH}(r)$ , as well as the velocity time autocorrelation function  $\Phi(t) = \langle \mathbf{V}(0) \cdot \mathbf{V}(t) \rangle$ . The calculation of such quantities at various time steps is also important for testing in our case, since it enables us to quantify sampling and dynamical accuracy. Note that the energy conservation is built in, to some extent, within the proposed approach. Hence, despite the fact that the total energy is not required to be conserved exactly (see the preceding paragraph), just the stability of its fluctuations might not guarantee a high accuracy overall.

The precision of the calculation of  $g_{OO}(r)$ ,  $g_{HH}(r)$ , and  $g_{OH}(r)$  was estimated using the normalized sum  $\Sigma = (\chi_{OO} + \chi_{HH} + \chi_{OH})/3$  of the three relative root-mean-square deviations  $\chi = (\int_0^{L/2} [g(r) - g_0(r)]^2 dr / \int_0^{L/2} g_0^2(r) dr)^{1/2}$  of  $g(r)$  from the “exact” counterparts  $g_0(r)$  corresponding to the OO, HH, and OH distribution functions. The “exact” values  $g_0(r)$  were precalculated employing the Verlet integrator (i.e., RESPA at  $n = 1$ ) with a small time step of  $h = 1$  fs and a long simulation length of  $t/h = 10^6$  to minimize any possible nu-

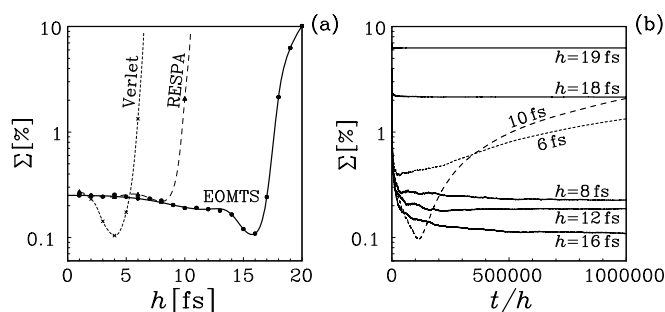


FIG. 3. Normalized deviations  $\Sigma$  of the radial distribution functions from their “exact” counterparts in the microcanonical MD simulations of the TIP4P water. The dependencies of  $\Sigma$  on the time step  $h$  (at fixed  $t/h = 10^6$ ) are plotted in (a) for the cases of the Verlet, RESPA, and EOMTS algorithms. The change in  $\Sigma$  with increasing the length  $t/h$  of the simulations is shown in (b) for the EOMTS integrator at a few fixed time steps  $h = 8, 12, 16, 18$ , and 19 fs. The short- and long-dashed curves in (b) correspond to the Verlet scheme at  $h = 6$  fs and the RESPA algorithm at  $h = 10$  fs.

merical uncertainties. The quantity  $\Sigma$  as a function of  $h$  and  $t$  is presented correspondingly in Figs. 3(a) and 3(b) for the Verlet, RESPA, and EOMTS algorithms. As can be seen, the EOMTS curves remain stable up to  $h \sim 16$  fs. Moreover, here no resonance appears at any intermediate values  $h < 16$  fs. Some decrease of  $\Sigma$  with increasing  $h$  in the range  $h \in [0, 16]$  fs can be explained by lowering of statistical noise (because at fixed  $t/h$ , the observation time  $t$  increases with rising  $h$ ). For the same reason, in the stability region the EOMTS values of  $\Sigma$  decrease with increasing  $t$  at fixed  $h$ . However, beginning from  $h \gtrsim 17$  fs, the function  $\Sigma(h)$  grows rapidly when  $h$  increases due to the MTS resonance. A similar behavior can be observed in the case of the RESPA and Verlet integrators, but at considerably smaller values of the time step, namely, at  $h \gtrsim 8$  fs and  $h \gtrsim 5$  fs, respectively. This confirms the conclusions made above when discussing the results of Figs. 1 and 2 on the energy conservation.

The first coordination numbers  $\frac{N}{V} \int_{r_1}^{r_2} 4\pi r^2 g(r) dr$  corresponding to the distribution functions  $g_{OO}(r)$ ,  $g_{HH}(r)$ , and  $g_{OH}(r)$  of the TIP4P water, obtained in the MD simulations by using the EOMTS algorithm, are shown in Fig. 4(a) with circles for many stepsizes from  $h = 1$  fs to  $h = 20$  fs in 1 fs interval. Here,  $r_1$  denotes the rightmost position starting from  $r = 0$  whereon  $g(r)$  is approximately zero, while  $r_2$  relates to the first minimum, i.e.,  $[r_1, r_2]$  is the region around the first peak of  $g(r)$ . We see that the coordination numbers are nearly independent of  $h$  in a wide range of values up to an order of  $h \sim 17$  fs. Slight deviations from the dashed horizontal lines (“exact results”) are caused by the statistical noise, which is non-zero because of the finiteness of the observation time  $t$ . Only at longer stepsizes of  $h \gtrsim 17$  fs, the deviations become too large due to the MTS instability, which is consistent with the results of Fig. 3. The example of the radial distribution functions  $g_{OO}(r)$ ,  $g_{HH}(r)$ , and  $g_{OH}(r)$  calculated in the EOMTS MD simulations with  $h = 16$  fs is presented with circles in Fig. 4(b), together with their “exact” counterparts (solid curves). The data related to the RESPA integrator with  $h = 10$  fs are shown as well, in order to demonstrate its clear inferiority with respect to the EOMTS integrator. It is readily seen that the deviations between the “exact” and RESPA

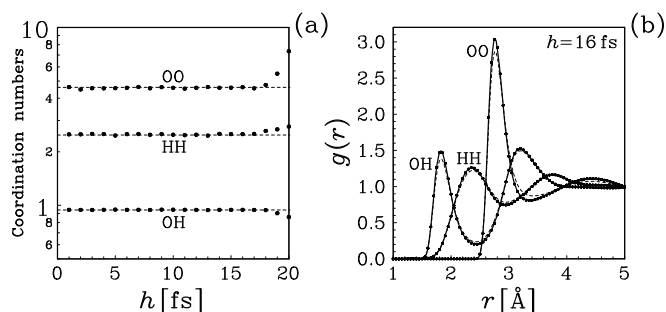


FIG. 4. The OO, HH, and OH coordination numbers obtained in the microcanonical MD simulations of the TIP4P water using the EOMTS method at various time steps  $h$  [circles in (a)], and the EOMTS radial distribution functions  $g_{OO}(r)$ ,  $g_{HH}(r)$ , and  $g_{OH}(r)$  calculated at  $h = 16$  fs [circles in (b)]. The “exact” results generated by the Verlet integrator with  $h = 1$  fs are plotted in (a) and (b) by the dashed horizontal lines and the solid curve, respectively. The dashed curve in (b) corresponds to the RESPA scheme at  $h = 10$  fs.

curves are big enough already at  $h = 10$  fs. At the same time, the EOMTS algorithm still continues to produce the radial functions with a high precision, even at a considerably larger step of  $h = 16$  fs.

The accuracy of the evaluation of the velocity time autocorrelation function  $\Phi(t)$  was measured in terms of the dimensionless root-mean-square deviations  $\Sigma_V = \frac{1}{\Phi_0(0)} (\int_0^{t_0} [\Phi(t) - \Phi_0(t)]^2 dt)^{1/2}$  of  $\Phi(t)$  from the “exact” counterpart  $\Phi_0(t)$ . Note that  $\Phi_0(t) \approx 0$  at  $t > t_0$ , where  $t_0 = 1$  ps, while  $\Phi_0(0) = 3k_B T / m_{\text{H}_2\text{O}}$  with  $k_B$  and  $m_{\text{H}_2\text{O}} = m_O + 2m_H$  being correspondingly the Boltzmann constant and the mass of the water molecule. The function  $\Phi_0(t)$ , like  $g_0(r)$ , was precisely precalculated using the Verlet integrator at  $h = 1$  fs. The dependency of  $\Sigma_V$  on  $h$  (at fixed  $t/h = 10^6$ ) is plotted in Fig. 5(a) for the cases of the Verlet, RESPA, and EOMTS integrators. Such a dependency is very similar to that concerning the radial distribution functions [see  $\Sigma(h)$  in Fig. 3(a)]. Indeed, the Verlet and RESPA algorithms again exhibit the instabilities already at relatively small steps of order  $h \gtrsim 5$  and 8 fs, respectively. At the same time, the EOMTS approach does not lose its precision up to  $h \sim 16$  fs. We see,

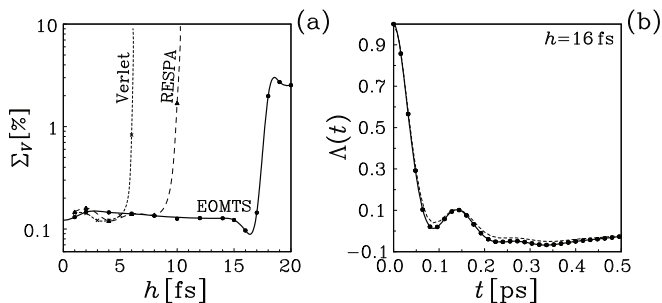


FIG. 5. The dimensionless deviations  $\Sigma_V$  of the velocity time autocorrelation function from its “exact” counterpart as depending on the size of the time step  $h$ , obtained in the microcanonical MD simulations of the TIP4P water employing the Verlet, RESPA, and EOMTS algorithms [see the corresponding symbols connected by the dashed or solid curves in (a)]. The normalized velocity time autocorrelation function related to the EOMTS integrator at  $h = 16$  fs is shown by circles in (b). The solid and dashed curves in (b) correspond to the “exact” result (Verlet with  $h = 1$  fs) and RESPA scheme (at  $h = 10$  fs), respectively.

therefore, that the estimations made on the basis of the relative total energy fluctuations  $\Upsilon$  [see Fig. 1] for the maximum allowable steps of the algorithms considered are in excellent accord with those followed from the real accuracies  $\Sigma$  and  $\Sigma_V$  of the observable quantities  $g(r)$  and  $\Phi(t)$ .

Finally, the normalized translational velocity time autocorrelation function  $\Lambda(t) = \Phi(t)/\Phi(0)$  of the TIP4P water, calculated in the EOMTS MD simulations at  $h = 16$  fs, is presented in Fig. 5(b) by circles in comparison with the “exact” data (solid curve) and the RESPA result at  $h = 10$  fs (dashed curve). As in the case of the radial functions [Fig. 4(b)], the deviations between the RESPA and “exact” curves are large enough already at  $h = 10$  fs. On the other hand, the EOMTS and “exact” results are practically indistinguishable, even at  $h = 16$  fs. We have also verified the fulfillment of the equipartition theorem by measuring the partial temperatures corresponding to translational and rotational degrees of freedom. Such temperatures were very close to the desired value  $T = 293$  K and the difference between them did not exceed 1% when  $h < 16$  fs. The absence of any artifacts within the stability region in the EOMTS quantities investigated above is due to the smallness of the virtual interactions used in the energy-targeted approach.

It is interesting to remark that the results obtained by the ERESPA and EOMTS algorithms appear to be almost independent, in the wide range  $1 \leq \kappa \lesssim 10$  on the number  $\kappa$  of outer time steps after which the virtual viscosity  $\lambda = \frac{1}{2\tau}(E - E_0)/K$  is updated. Thus, the total computational costs can be made nearly the same as in the case of the RESPA scheme. For instance, the overhead on the calculation of the full energy  $E$  decreases from 25% to 5% when  $\kappa$  increases from 1 to 5. In addition, it has been realized that all the calculated quantities presented in Figs. 1–5 for  $\kappa = 1$  are not affected by such an increase. As an example, the function  $\Upsilon(h)$  corresponding to the EOMTS algorithm with  $\kappa = 5$  is shown in Fig. 1 by the long dashed thin curve. It lies very close to the solid curve related to the case  $\kappa = 1$ .

Note also that the barrier  $h \sim 16$  fs can be shifted to larger values using more aggressive rescaling of translational and angular momenta. This can be done by decreasing the virtual relaxation time down to  $\tau = h$ . However, in such a case, despite the achieved stability in the conservation of the total energy, the observable quantities will significantly differ from their “exact” values. Moreover, the equipartition theorem will then be violated, leading to too large deviations between the partial temperatures. On the other hand, the maximal allowable steps can be enlarged by increasing the cutoff radius  $r_c$  (then  $\gamma$  increases as well). But, this inflates the calculation cost of the short-ranged interactions, reducing the efficiency of the MTS integration.

## IV. CONCLUSION

In summary, we have developed a novel multiple time step approach to avoid the resonance instabilities in microcanonical MD simulations. It combines a new energy-constrained technique with a generalization of the phase-transforming scheme to the case when not only translational but also rotational degrees of freedom are presented in the

system. As demonstrated for water, the proposed approach allows one to considerably increase the size of the MD time step in comparison with the standard microcanonical MTS schemes. Such an increase gives the possibility to reduce the number of expensive long-ranged force and torque recalculations when integrating the equations of motion, leading to a speedup of the MD simulations. Moreover, the new algorithms derived are explicit and able to exactly reproduce the structures of rigid molecular segments without involving any iteration procedures, thus further improving the efficiency of the MD computations.

## ACKNOWLEDGMENTS

We gratefully acknowledge the support by the National Academy of Sciences of Ukraine (I.P.O.) and by the National Research Council (NRC) of Canada (A.K.).

- <sup>1</sup>J. U. Brackbill and B. I. Cohen, *Multiple Time Scales* (Academic, Orlando, 1985).
- <sup>2</sup>M. P. Allen and D. J. Tildesley, *Computer Simulation of Liquids* (Clarendon, Oxford, 1987).
- <sup>3</sup>D. Frenkel and B. Smit, *Understanding Molecular Simulation: From Algorithms to Applications* (Academic, New York, 1996).
- <sup>4</sup>C. K. R. T. Jones and A. I. Khibnik, *Multiple-Time-Scale Dynamical Systems* (Springer-Verlag, Berlin, 2001).
- <sup>5</sup>A. S. Lipatov, *The Hybrid Multiscale Simulation Technology* (Springer, Berlin, 2002).
- <sup>6</sup>B. Leimkuhler and S. Reich, *Simulating Hamiltonian Dynamics* (Cambridge University Press, Cambridge, England, 2005).
- <sup>7</sup>W. B. Streett, D. J. Tildesley, and G. Saville, *Mol. Phys.* **35**, 639 (1978).
- <sup>8</sup>R. D. Swindoll and J. M. Haile, *J. Comput. Phys.* **53**, 289 (1984).
- <sup>9</sup>O. Teleman and B. Jönsson, *J. Comput. Chem.* **7**, 58 (1986).
- <sup>10</sup>M. E. Tuckerman, G. J. Martyna, and B. J. Berne, *J. Chem. Phys.* **93**, 1287 (1990).
- <sup>11</sup>M. E. Tuckerman, B. J. Berne, and A. Rossi, *J. Chem. Phys.* **94**, 1465 (1991).
- <sup>12</sup>M. E. Tuckerman, B. J. Berne, and G. J. Martyna, *J. Chem. Phys.* **94**, 6811 (1991).
- <sup>13</sup>T. Forester and W. Smith, *Mol. Simul.* **13**, 195 (1994).
- <sup>14</sup>H. Grubmüller, H. Heller, A. Windemuth, and K. Schulten, *Mol. Simul.* **6**, 121 (1991).
- <sup>15</sup>M. E. Tuckerman, B. J. Berne, and G. J. Martyna, *J. Chem. Phys.* **97**, 1990 (1992).
- <sup>16</sup>S. J. Stuart, R. Zhou, and B. J. Berne, *J. Chem. Phys.* **105**, 1426 (1996).
- <sup>17</sup>A. Kopf, W. Paul, and B. Dünweg, *Comput. Phys. Commun.* **101**, 1 (1997).
- <sup>18</sup>J. A. Izaguirre, D. P. Catarello, J. M. Wozniak, and R. D. Skeel, *J. Chem. Phys.* **114**, 2090 (2001).
- <sup>19</sup>R. D. Skeel and J. A. Izaguirre, *Mol. Phys.* **100**, 3885 (2002).
- <sup>20</sup>S. Melchionna, *J. Chem. Phys.* **127**, 044108 (2007).
- <sup>21</sup>G. Zhang and T. Schlick, *J. Comput. Chem.* **14**, 1212 (1993).
- <sup>22</sup>G. Zhang and T. Schlick, *J. Chem. Phys.* **101**, 4995 (1994).
- <sup>23</sup>T. Schlick, E. Barth, and M. Mandziuk, *Annu. Rev. Biophys. Biomol. Struct.* **26**, 181 (1997).
- <sup>24</sup>E. Barth and T. Schlick, *J. Chem. Phys.* **109**, 1617 (1998).
- <sup>25</sup>B. Garcia-Archilla and R. D. Skeel, *SIAM J. Sci. Comput. (USA)* **20**, 930 (1998).
- <sup>26</sup>J. A. Izaguirre, S. Reich, and R. D. Skeel, *J. Chem. Phys.* **110**, 9853 (1999).
- <sup>27</sup>Q. Ma and J. A. Izaguirre, *Multiscale Model. Simul.* **2**, 1 (2003).
- <sup>28</sup>G. J. Martyna, M. E. Tuckerman, D. J. Tobias, and M. L. Klein, *Mol. Phys.* **87**, 1117 (1996).
- <sup>29</sup>A. Cheng and K. M. Merz, Jr., *J. Phys. Chem. B* **103**, 5396 (1999).
- <sup>30</sup>J. Komeiji, *J. Mol. Struct.: THEOCHEM* **530**, 237 (2000).
- <sup>31</sup>P. Minary, G. J. Martyna, and M. E. Tuckerman, *J. Chem. Phys.* **118**, 2510 (2003).
- <sup>32</sup>S. A. Chin, *J. Chem. Phys.* **120**, 8 (2004).
- <sup>33</sup>P. Minary, M. E. Tuckerman, and G. J. Martyna, *Phys. Rev. Lett.* **93**, 150201 (2004).
- <sup>34</sup>J. B. Abrams, M. E. Tuckerman, and G. J. Martyna, *Computer Simulations in Condensed Matter Systems: From Materials to Chemical Biology*, Lecture Notes in Physics Vol. 703, p. 139 (Springer-Verlag, Berlin, 2006), Vol. 1.
- <sup>35</sup>I. P. Omelyan, *J. Chem. Phys.* **131**, 104101 (2009).
- <sup>36</sup>R. Zhou and B. J. Berne, *J. Chem. Phys.* **103**, 9444 (1995).
- <sup>37</sup>M. Watanabe and M. Karplus, *J. Phys. Chem.* **99**, 5680 (1995).
- <sup>38</sup>E. Barth and T. Schlick, *J. Chem. Phys.* **109**, 1633 (1998).
- <sup>39</sup>M. Mandziuk and T. Schlick, *Chem. Phys. Lett.* **237**, 525 (1995).
- <sup>40</sup>T. Schlick, M. Mandziuk, R. D. Skeel, and K. Srinivas, *J. Comput. Phys.* **140**, 1 (1998).
- <sup>41</sup>G. Ciccotti, J. P. Ryckaert, and M. Ferrario, *Mol. Phys.* **47**, 1253 (1982).
- <sup>42</sup>H. C. Andersen, *J. Comput. Phys.* **52**, 24 (1983).
- <sup>43</sup>A. Kol, B. B. Laird, and B. J. Leimkuhler, *J. Chem. Phys.* **107**, 2580 (1997).
- <sup>44</sup>A. Dullweber, B. Leimkuhler, and R. McLachlan, *J. Chem. Phys.* **107**, 5840 (1997).
- <sup>45</sup>I. P. Omelyan, *Comput. Phys.* **12**, 97 (1998).
- <sup>46</sup>I. P. Omelyan, *Comput. Phys. Commun.* **109**, 171 (1998).
- <sup>47</sup>I. P. Omelyan, *Phys. Rev. E* **58**, 1169 (1998).
- <sup>48</sup>N. Matubayasi and M. Nakahara, *J. Chem. Phys.* **110**, 3291 (1999).
- <sup>49</sup>I. P. Omelyan, *Mol. Simul.* **22**, 213 (1999).
- <sup>50</sup>T. F. Miller III, M. Eleftheriou, P. Pattnaik, A. Ndirango, D. Newns, and G. J. Martyna, *J. Chem. Phys.* **116**, 8649 (2002).
- <sup>51</sup>I. P. Omelyan, *J. Chem. Phys.* **127**, 044102 (2007).
- <sup>52</sup>I. P. Omelyan, *Phys. Rev. E* **78**, 026702 (2008).
- <sup>53</sup>W. Shinoda and M. Mikami, *J. Comput. Chem.* **24**, 920 (2003).
- <sup>54</sup>C. Sagui and T. A. Darden, *Annu. Rev. Biophys. Biomol. Struct.* **28**, 155 (1999).
- <sup>55</sup>W. L. Jorgensen, J. Chandrasekhar, J. D. Madura, R. W. Impey, and M. L. Klein, *J. Chem. Phys.* **79**, 926 (1983).
- <sup>56</sup>H. J. C. Berendsen, J. R. Grigera, and T. P. Straatsma, *J. Phys. Chem.* **91**, 6269 (1987).
- <sup>57</sup>P. J. Steinbach and B. R. Brooks, *J. Comput. Chem.* **15**, 667 (1994).
- <sup>58</sup>K. Toukan and A. Rahman, *Phys. Rev. B* **31**, 2643 (1985).
- <sup>59</sup>D. Case, T. Cheatham, T. Darden, H. Gohlke, R. Luo, K. Merz, A. Onufriev, C. Simmerling, B. Wang, and R. Woods, *J. Comput. Chem.* **26**, 1668 (2005).
- <sup>60</sup>G. A. Kaminski, R. A. Friesner, J. Tirado-Rives, and W. L. Jorgensen, *J. Phys. Chem. B* **105**, 6474 (2001).
- <sup>61</sup>A. D. MacKerell, Jr., D. Bashford, M. Bellott, R. L. Dunbrack, Jr., J. D. Evanseck, M. J. Field, S. Fischer, J. Gao, H. Guo, S. Ha, D. Joseph-McCarthy, L. Kuchnir, K. Kuczera, F. T. K. Lau, C. Mattos, S. Michnick, T. Ngo, D. T. Nguyen, B. Prodhom, W. E. Reiher III, B. Roux, M. Schlenkrich, J. C. Smith, R. Stote, J. Straub, M. Watanabe, J. Wiórkiewicz-Kuczera, D. Yin, and M. Karplus, *J. Phys. Chem. B* **102**, 3586 (1998).
- <sup>62</sup>M. Christen, P. H. Hünenberger, D. Bakowies, R. Baron, R. Bürgi, D. P. Geerke, T. N. Heinz, M. A. Kastholz, V. Kräutler, C. Oostenbrink, C. Peter, D. Trzesniak, and W. F. van Gunsteren, *J. Comput. Chem.* **26**, 1719 (2005).
- <sup>63</sup>H. F. Trotter, *Proc. Amer. Math. Soc.* **10**, 545 (1959).
- <sup>64</sup>W. C. Swope, H. C. Andersen, P. H. Berens, and K. R. Wilson, *J. Chem. Phys.* **76**, 637 (1982).
- <sup>65</sup>I. P. Omelyan, I. M. Mryglod, and R. Folk, *Phys. Rev. E* **65**, 056706 (2002).
- <sup>66</sup>R. van Zon and J. Schofield, *Phys. Rev. E* **75**, 056701 (2007).
- <sup>67</sup>R. Kutteh, *J. Chem. Phys.* **111**, 1394 (1999).
- <sup>68</sup>K. Hermansson, G. C. Lie, and E. Clementi, *J. Comput. Chem.* **9**, 200 (1988).
- <sup>69</sup>S. C. Harvey, R. K.-Z. Tan, and T. E. Cheatham III, *J. Comput. Chem.* **19**, 726 (1998).
- <sup>70</sup>H. J. C. Berendsen, J. P. M. Postma, W. F. v. Gunsteren, A. DiNola, and J. R. Haak, *J. Chem. Phys.* **81**, 3684 (1984).
- <sup>71</sup>A. Mudia and C. Chakravarty, *Mol. Phys.* **102**, 681 (2004).
- <sup>72</sup>G. Bussi, D. Donadio, and M. Parrinello, *J. Chem. Phys.* **126**, 014101 (2007).
- <sup>73</sup>I. P. Omelyan, *Comput. Phys. Commun.* **107**, 113 (1997).
- <sup>74</sup>R. Zhou, E. Harder, H. Xu, and B. J. Berne, *J. Chem. Phys.* **115**, 2348 (2001).
- <sup>75</sup>X. Qian and T. Schlick, *J. Chem. Phys.* **116**, 5971 (2002).
- <sup>76</sup>G. Han, Y. Deng, J. Glimm, and G. Martyna, *Comput. Phys. Commun.* **176**, 271 (2007).
- <sup>77</sup>J. A. Morrone, R. Zhou, and B. J. Berne, *J. Chem. Theory Comput.* **6**, 1798 (2010).